# Improvements in Silicon Oxide Dielectric Loss for Superconducting Microwave Detector Circuits

Dale Li, J. Gao, J. E. Austermann, J. A Beall, D. Becker, H.-M. Cho, A. E. Fox, N. Halverson, J. Henning, G. C. Hilton, J. Hubmayr, K. D. Irwin, J. Van Lanen, J. Nibarger, and M. Niemack

***Abstract*—Dielectric loss in low-temperature superconducting integrated circuits can cause lower overall efficiency, particularly in the 90 to 220 GHz regime. We present a method to tune the dielectric loss for silicon oxide deposited by plasma-enhanced chemical-vapor deposition at ambient temperatures. Deposition in an environment with a higher silane-to-oxygen ratio produces silicon oxide films with a lower loss-tangent and a slightly higher optical index of refraction, while contributing no appreciable change in film stress. We measured the dielectric loss by fabricating a series of Nb-$SiO_x$-Nb microstrip resonators in the frequency range of 6 to 9 GHz and comparing their temperature dependence to a model of parasitic two-level-system fluctuators. The dielectric loss-tangent of silicon oxide was improved from $6 \times 10^{-3}$ for stoichiometric silicon dioxide to $2 \times 10^{-3}$ for a more silicon-rich silicon oxide. We present details of the fabrication process and measurements of microstrip resonators.**

***Index Terms*—Dielectric, efficiency, loss-tangent, microwave resonators, plasma-enhanced chemical-vapor deposition (PECVD), silicon oxide.**

## I. Introduction

SILICON oxide is a ubiquitous insulating material used in superconducting circuits and valued for its stability and relative low film-stress. It can be deposited amorphously by sputtering, electron beam evaporation, or by electron-cyclotron-resonance plasma-enhanced chemical-vapor deposition (ECR-PECVD) [1], [2]. With ECR-PECVD, deposition parameters such as stoichiometry, temperature, voltage, power, and pressure can all be carefully controlled, making it possible to deposit silicon oxide films with different characteristics.

One characteristic of unique importance to superconducting integrated circuits is dielectric loss, which has been correlated to the presence of parasitic two-level-system (TLS) fluctuators in the insulator material. Much theoretical and experimental progress has already been made in understanding TLS loss mechanisms [3], [4]. However, until recently, it was assumed that deposition of stoichiometric silicon dioxide ($SiO_2$) would be the most stable and lowest-loss silicon oxide film [1], [2]. However, studies in the ECR-PECVD deposition of silicon nitride have shown that more silicon-rich films can exhibit much lower loss than nitrogen-rich films in microwave resonators [5]. Unfortunately silicon nitride films exhibit very high stress, which precludes its use in devices with relieved membranes or micro electro-mechanical systems (MEMS). We applied a similar approach to reduce loss in silicon oxide by attempting to deposit a more silicon-rich film. We present a series of measurements of Nb-$SiO_x$-Nb microstrip resonators that show an inverse correlation between the electromagnetic dissipation-parameter measured as a loss-tangent and the silane-to-oxygen flow-rate ratio used during deposition.

Manuscript received October 9, 2012; accepted January 14, 2013. Date of publication January 24, 2013; date of current version February 25, 2013.

Dale Li, J. Gao, J. A. Beall, D. Becker, H.-M. Cho, A. E. Fox, G. C. Hilton, J. Hubmayr, K. D. Irwin, J. Van Lanen, J. Nibarger, and M. Niemack are in the Quantum Electronics and Photonics Division, National Institute of Standards and Technology, Boulder, CO 80305 USA (e-mail: dale.li@boulder.nist.gov).

J. E. Austermann, N. Halverson, and J. Henning are with the Department of Physics, University of Colorado, Boulder, CO 80309 USA.

Color versions of one or more of the figures in this paper are available online at http://ieeexplore.ieee.org.

Digital Object Identifier 10.1109/TASC.2013.2242951

## II. Dielectric Loss and Optical Efficiency

Feedhorn-coupled, superconducting-polarimeters designed to measure the Cosmic Microwave Background (CMB) often have microstrip lines that span across low-stress membranes and operate at a frequency range of 90 GHz to 220 GHz with low noise and low excitation power [6], [7]. In this regime, unwanted dielectric loss in microstrips and integrated filters can lead to a detrimental decrease of the coupling efficiency of these detectors to the CMB.

Fig. 1 is a photograph of a recent CMB detector pixel designed and fabricated at the National Institute of Standards and Technology (NIST). This pixel is a polarimeter design with separate channels for $x$ and $y$ polarizations. Light couples through optical elements and enters a corrugated silicon feedhorn [6], [7]; from there it is guided to the triangular fins in the center of the pixel. These triangular fins, called ortho-mode transducers (OMT), then couple to a coplanar waveguide (CPW), a transition element, a microstrip waveguide, a series of integrated bandpass filters, an additional microstrip waveguide, and finally couple to and terminate in a gold meander located on an island with a transition edge sensor (TES).

The total simulated efficiency for the CMB detector design excluding any dielectric loss is 80% to 90%. However, fabrication of these designs with stoichiometric silicon dioxide (silane-to-oxygen flow-rate ratio 6.4) yielded detectors with a total measured optical efficiency of 57% ($\pm$4% statistical and $\pm$9% systematic error) [8]. Dielectric loss can lead to this discrepancy between the simulated efficiency and the measured efficiency.

Fig. 2 shows the result of a finite-element analysis where the dielectric loss-tangent is varied, producing an appreciable change in total detector efficiency for two different detector designs. The green curve is simulated for a design very close to Fig. 1 and the original prototype for the South Pole Telescope polarimeters. In removing the band-pass filters and shortening the length of the microstrip feed lines by 47%, the blue line shows that a much higher total efficiency is achievable for all values of dielectric loss-tangent. For dielectric films with a loss-tangent of $6 \times 10^{-3}$, merely changing the design can increase the optical efficiency from $\sim$55% to $\sim$80%.

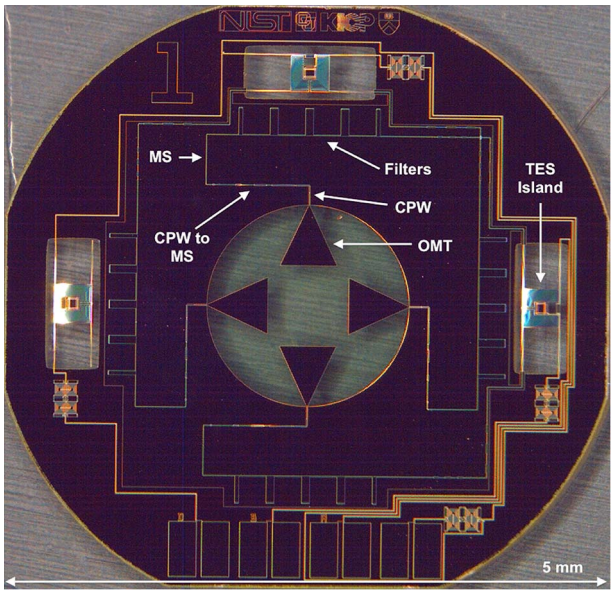


Fig. 1. CMB5 single-pixel superconducting polarimeter prototype. The triangular fins in the center of the pixel are the ortho-mode transducers (OMTs) that couple incoming photons to a coplanar waveguide (CPW), to transition elements to a microstrip transmission line (MS), to bandpass filters, and terminate at a transition to a gold meander on the transition edge sensor (TES) islands. The optical efficiency at 150 GHz for this design, with stoichiometric silicon dioxide used in the microstrips and filters, has been measured between 40 and 60%.

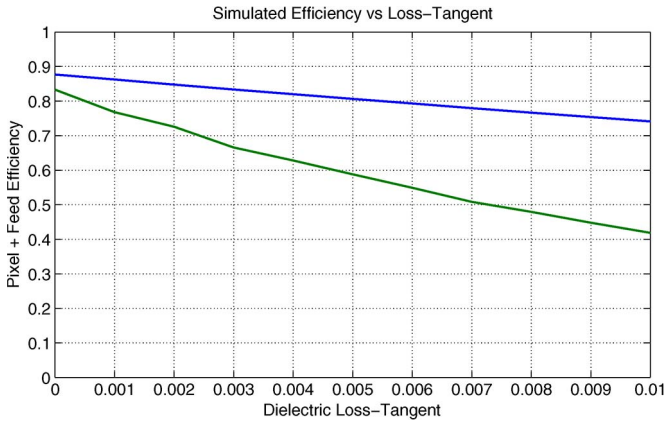


Fig. 2. Simulation predictions for the change in total optical efficiency at 150 GHz of detectors with corrugated feedhorns. The green line is simulated for a detector design similar to the one shown in Fig. 1. Removing the band-pass filters and reducing the microstrip length by 47% gives the blue simulated curve used for the design of the South Pole Telescope polarimeters.

Improvement in the dielectric loss tangent would produce a further gain in efficiency even for detector designs that include an integrated band-pass filter.

## III. Measurement of Microstrip Resonators

Since the CMB detectors are complex circuits with many fabrication steps and are designed to operate at 150 GHz, it is cost-prohibitive to use full-scale detector pixels for efficiency testing and fabrication feedback. However, because loss due to TLS fluctuators has been observed at millimeter wavelengths ($< 100$ GHz) [9], we made the hypothesis that reducing the TLS loss-tangent at the range of 6 GHz to 9 GHz may also reduce the TLS loss-tangent at 150 GHz, and thus increase the efficiency.

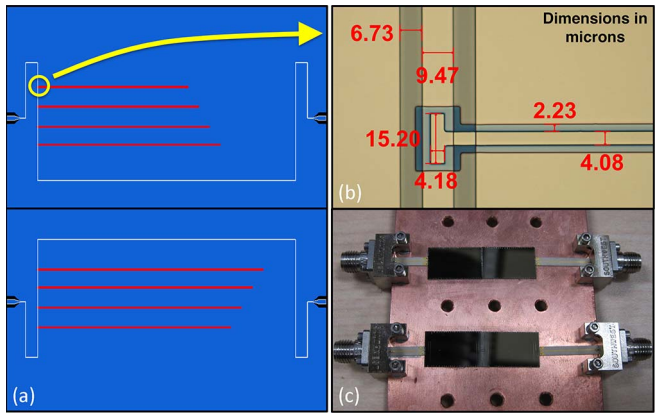


Fig. 3. Microstrip resonator designs. (a) Two chips were designed with four $\lambda/2$ open microstrip resonators each. The top chip, style "A", has resonances centered about 8.25 GHz while the bottom chip, style "B", has resonances centered about 6.25 GHz. The chips are $9.5 \times 15$ mm$^2$. (b) Micrograph at 100 times magnification shows how the microstrip resonators are capacitively coupled to the CPW transmission line. (c) Photograph of four chips bonded to a copper plate with microwave feed lines transitioning to SMA connectors.

To test this hypothesis, we designed a series of Nb-$SiO_x$-Nb microstrip resonators and measured their TLS loss-tangent in the frequency range of 6 GHz to 9 GHz. We then deposited the lowest-loss dielectric into actual CMB detectors and measured the coupling efficiencies at 150 GHz.

The microstrip resonator design is shown in Fig. 3. Two chips were designed with four microstrip resonators each, centered at different frequencies. Style "A" chips have resonances centered about 8.25 GHz, while style "B" chips have resonances centered about 6.25 GHz. Note that the resonance frequencies also depend on the dielectric constant of the insulator and can vary with the silicon oxide deposition parameters. We fabricated both style "A" and style "B" chips on a single wafer. Subsequently, each wafer was fabricated with a different set of silicon oxide deposition parameters. Two chips can be cooled together in one continuous feed line since the set of frequencies from style "A" and style "B" chips do not overlap.

The resonator chips were mounted to a copper backing plate and wire-bonded to gold microwave circuit-board feed lines. End-launch SMA connectors [as shown in Fig. 3(c)] were then clamped to the circuit-board feed lines. Typical microwave components were used in the measurement including a high electron mobility transistor (HEMT) microwave amplifier, microwave circulator, and network analyzer. The samples were cooled by use of a dry adiabatic-demagnetization refrigerator (ADR), which enables stable temperature control from 100 mK to 10 K.

A typical transmission spectrum $(S_{21})$ of one style "A" and one style "B" resonator chip bonded in series is shown in Fig. 4. The eight resonance lines are easily separable and identifiable for the two different microstrip resonator designs. Although there are additional resonance lines in the spectrum, only the microstrip resonances shift with temperature (or microwave power); therefore the static lines can be ignored in the analysis.

The temperature dependance of a set of style "B" microstrip resonators is shown in Fig. 5 (style "A" chips produce a similar result for the same dielectric). Measurement of intrinsic dielectric loss can be made by either reducing the microwave drive power at a fixed temperature and extrapolating the quality factor at zero power, or by reducing the temperature at a fixed

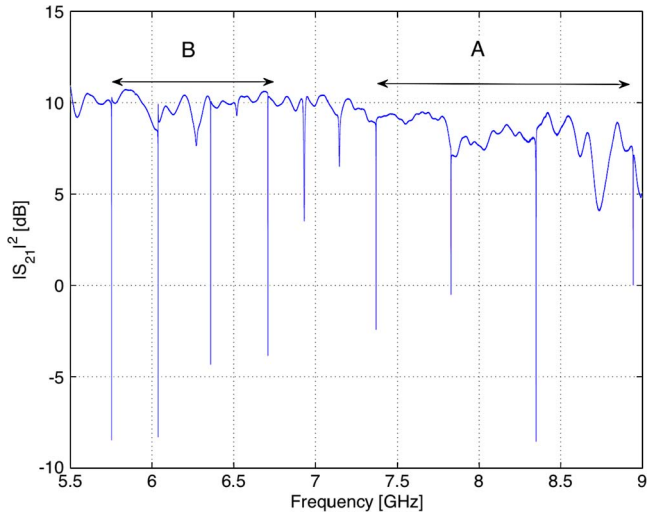


Fig. 4. Uncalibrated transmission measurement ($S_{21}$) of two microstrip resonator chips bonded in series. Four resonance dips centered around 8.25 GHz are from an "A" style resonator chip, while four resonance dips centered around 6.25 GHz are from a "B" style resonator chip. Other resonance dips are visible in this frequency window due to stray inductance and capacitance of the microwave setup, but these resonances can be ignored since their resonance frequencies are independent of temperature.

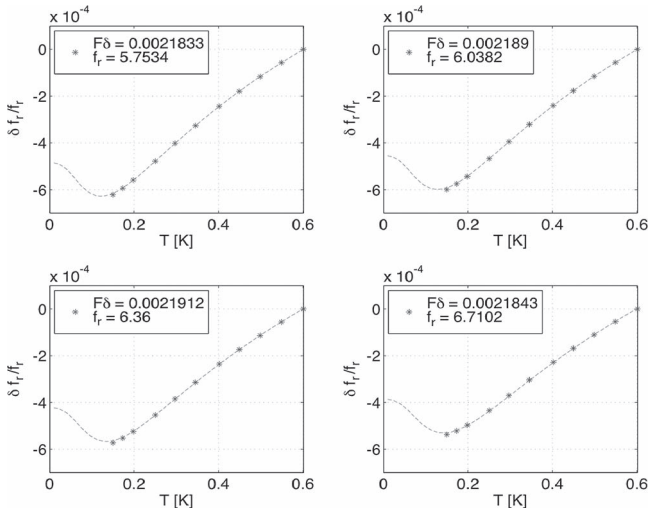


Fig. 5. Temperature dependencies of a style "B" microstrip resonator chip. Driving the microwave resonances at a fixed moderate power gives a high signal-to-noise ratio but begins to appreciably heat the sample at lower temperatures ($< 0.1$ K), where the cooling power of the refrigerator drops. Fitting the temperature dependence to (1) gives the minimum resonance frequency, $f_r$ and the loss-tangent, $F\delta$ (for filling factor near unity).

microwave drive power and extrapolating the loss-tangent at zero temperature [3], [10]–[12]. The latter strategy is preferred because of the high signal-to-noise ratio achievable (less averaging) and fast temperature stabilization of an ADR. One caveat is that at lower temperatures, the microwave power may begin to heat the sample, since the cooling power of the ADR drops at the base temperature.

The resulting temperature dependency of the frequency can be modeled by

$$\frac{\delta f_r}{f_r} = \frac{F\delta^0_{TLS}}{\pi}\left[\mathrm{Re}\,\Psi\left(\frac{1}{2}+\frac{hf_r}{2\pi j k_B T}\right) - \log\frac{hf_r}{2\pi k_B T}\right] \quad (1)$$

where $f_r$ is the resonance frequency, $\delta f_r = f_r(T) - f_r(0)$, T is the temperature, F is the filling factor of the dielectric within the microstrip, $\delta^0_{TLS}$ is the intrinsic zero-temperature loss-tangent of the dielectric due to parasitic two-level-system fluctuators, $k_B$ is Boltzmann's constant, $h$ is Planck's constant, and $\Psi(x) = \Gamma'(x)/\Gamma(x)$ is the digamma function for complex argument $x$ [3], [4], [10]–[12]. The filling factor of a microstrip resonator is very close to unity, so $F\delta^0_{TLS}$ gives the loss-tangent for the deposited dielectric. Fig. 5 shows a fit of (1) to microstrip resonator data yielding a loss-tangent as a fit parameter.

The microstrip resonator chips consist of three deposited layers: 200 nm of sputtered Nb (the feed line and ground plane), 350 nm of silicon oxide (insulator), and 300 nm of sputtered Nb (top wiring of microstrip). Since the critical temperature of Nb is 9.2 K, the kinetic inductance remains flat below 1 K. The temperature dependance of the resonant frequency of the microstrips are then dominated by a change in TLS dynamics in the dielectric. Poor quality Nb films, however, can occur from corrosion of the sputter target, or other contaminants in the deposition chamber. These poor quality Nb films can exhibit a lower critical temperature than pure Nb, and can result in temperature dependence of the kinetic inductance and a poor fit to (1). Qualitatively, this deviation to the fitting curve can appear as a slight downturn of the frequency versus temperature curve at temperatures near and above 1 K.

## IV. Tuning Silicon Oxide Deposition Parameters

The idea of depositing a silicon-based insulator in a silicon-rich environment has been successfully applied to silicon nitride films for use in superconducting qubit experiments [5]. In those experiments, the loss-tangent was reduced by almost a factor of 50 between higher-loss silicon nitride films deposited in a nitrogen-rich environment $(1.2 \times 10^{-3})$ and lower-loss silicon nitride films deposited in a silicon-rich environment $(2.5 \times 10^{-5})$. The drawback, however, was an accompanying increase in film stress by over an order of magnitude (as high as 1200 MPa). For CMB detectors with very delicate membranes, high film-stress is undesirable.

The ECR-PECVD deposition of silicon oxide was adjusted to produce silicon oxide films in silicon-rich environments. Fig. 6 (top left) shows the fitted loss-tangent at 6 GHz to 9 GHz [from (1)] to fabricated microstrip resonators as a function of silane-to-oxygen flow-rate ratio during deposition. The optical index of refraction and the deposition rate were measured at room temperature by use of an ellipsometer (measured at optical wavelengths: 6328 Å, 8260 Å, and 12880 Å). The film stress was measured by a change in optical deflection by use of a stress gauge. Although the deposition rate was observed to decrease with increased silane-to-oxygen flow-rate ratio, the film stress remained compressive between 50 MPa and 150 MPa.

There is a strong correlation between the room-temperature-measured optical index of refraction of silicon oxide films and the loss-tangent measured at 6 GHz to 9 GHz and 150 GHz. For a silane-to-oxygen flow-rate ratio of 13.1 (131 sccm $SiH_4$, 10 sccm $O_2$) microstrip resonators were fabricated and measured with a loss-tangent of $2 \times 10^{-3}$ and CMB detectors were fabricated and measured with a total optical efficiency of $\sim$91% [13]. The CMB detector designs also removed the band-pass filters from the earlier CMB5 and CMB6-2 designs, and

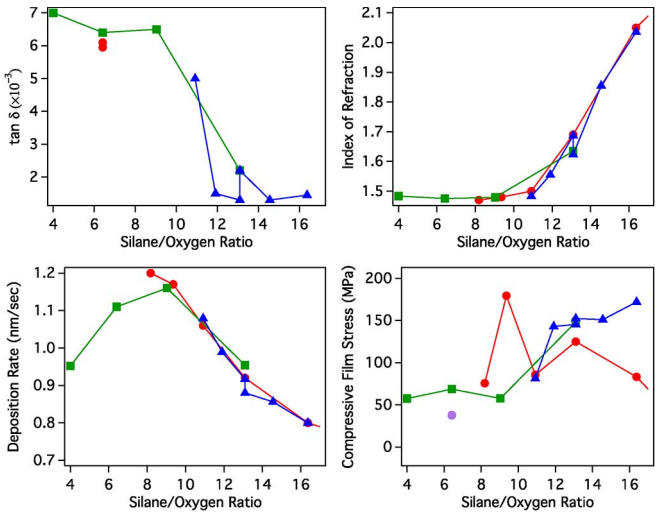


Fig. 6. For Nb-$SiO_x$-Nb microstrip resonators from 6 to 9 GHz with different silane-to-oxygen flow-rate ratio depositions: (a) dielectric loss-tangent, (b) optical index of refraction, (c) deposition rate, and (d) compressive film stress. Flow-rate ratios as high as 65.5 were measured in blank silicon oxide films with an optical index of 2.89 but were not implemented in a microstrip resonator test due to reduced adhesion to Nb at silane/oxygen ratios above 20. Stoichiometric silicon dioxide is deposited with a silane-to-oxygen ratio of 6.4. Different colored symbols represent different fabrication runs.

shortened the microstrip sections by 47% to reduce the amount of insulator in the design. The full compliment of these detector arrays were deployed to the South Pole Telescope and currently in use for observation of the polarization of the CMB.

Silane-to-oxygen flow-rate ratios above 16 and up to 65.5 were also used to deposit silicon oxide films on blank silicon substrate wafers. For these very high silicon-rich depositions, the deposition rate dropped and tapered to 0.6 nm/sec, while the optical index of refraction increased and tapered to 2.8. Even for these very high silicon-rich depositions the film stress was measured between 50 MPa and 150 MPa. However, for silicon oxide films deposited with silane-to-oxygen ratios above 20, adhesion to Nb was greatly reduced and films began to bubble and peel immediately after deposition.

## V. Conclusion

For fabrication of sensitive CMB detectors, silicon oxide can be deposited in a slightly more silicon-rich environment, which produces a film with higher optical index of refraction and lower dielectric loss-tangent. Measurements of microstrip resonators at 6 GHz to 9 GHz show a temperature dependence of microstrip resonant frequencies, which agree well with an analytical model assuming loss due only to parasitic two-level-system fluctuators. Silicon oxide films deposited by ECR-PECVD with a silane-to-oxygen flow-rate ratio of 13.1 were incorporated into a full compliment of CMB polarimeter arrays fabricated for the South Pole Telescope. Optical efficiency measurements report a total detector coupling efficiency of ∼91%. We estimate a gain of ∼25% in coupling efficiency due to a reduction of insulator in the detector design with another gain of ∼10% in coupling efficiency due to the decrease of loss-tangent in the silicon-rich silicon oxide film. By utilizing the improved dielectric loss-tangent, future detector designs could include integrated band-pass filters and maintain an optical efficiency from 70% to 80%.

## Acknowledgment

The authors would like to thank the TRUCE collaboration and the SPTpol collaboration.

## References

[1] G. Lucovsky, P. D. Richard, D. V. Tsu, S. Y. Lin, and R. J. Markunas, "Deposition of silicon dioxide and silicon nitride by remote plasma enhanced chemical vapor deposition," *J. Vac. Sci. Technol. A*, vol. 4, no. 3, pp. 681–688, May 1986.

[2] J. E. Sauvageau, C. J. Burroughs, M. W. Cromar, and J. A. Koch, "Optimization of ECR-based PECVD oxide films for superconducting integrated circuit fabrication," in *Proc. 37th Soc. Vac. Coaters Annu. Tech. Conf.*, 1994, pp. 383–388.

[3] J. Gao, "The physics of superconducting microwave resonators," M.S. thesis, Dept. Phys., Caltech, Pasadena, CA, USA, May, 2008, pp. 95-126.

[4] D. P. Pappas, M. R. Vissers, D. S. Wisbey, J. S. Kline, and J. Gao, "Two level system loss in superconducting microwave resonators," *IEEE Trans. Appl. Supercond.*, vol. 21, no. 3, pp. 871–874, Jun. 2011.

[5] H. Paik and K. D. Osborn, "Reducing quantum-regime dielectric loss of silicon nitride for superconducting quantum circuits," *Appl. Phys. Lett.*, vol. 96, no. 7, pp. 072505-1–072505-3, Feb. 2010.

[6] J. Hubmayr, J. W. Appel, J. E. Austermann, J. A. Beall, D. Becker, B. A. Benson, L. E. Bleem, J. E. Carlstrom, C. L. Chang, H. M. Cho, A. T. Crites, T. Essinger-Hileman, A. Fox, E. M. George, N. W. Halverson, N. L. Harrington, J. W. Henning, G. C. Hilton, W. L. Holzapfel, K. D. Irwin, A. T. Lee, D. Li, J. McMahon, J. Mehl, T. Natoli, M. D. Niemack, L. B. Newburgh, J. P. Nibarger, L. P. Parker, B. L. Schmitt, S. T. Staggs, J. Van Lanen, E. J. Wollack, and K. W. Yoon, "An all silicon feedhorn-coupled focal plane for cosmic microwave background polarimetry," *J. Low Temp. Phys.*, vol. 167, no. 5/6, pp. 904–910, Jun. 2012.

[7] M. D. Niemack, J. Beall, D. Becker, H.-M. Cho, A. Fox, G. Hilton, J. Hubmayr, K. Irwin, D. Li, J. McMahon, J. Nibarger, and J. Van Lanen, "Optimizing feedhorn-coupled TES polarimeters for balloon and space-based CMB observations," *J. Low Temp. Phys.*, vol. 167, no. 5/6, pp. 917–922, Jun. 2012.

[8] J. W. Henning, J. W. Appel, J. E. Austermann, J. A. Beall, D. Becker, D. Bennett, A. Bleem, L. E. Benson, B. A. Britton, J. Carlstrom, J. E. Chang, C. L. Cho, H. M. Crites, A. T. Essinger-Hileman, T. Everett, W. George, E. M. Halverson, N. W. Hilton, G. C. Holzapfel, W. L. Hubmayr, J. Irwin, K. D. Li, D. McMahon, J. Mehl, J. Meyer, S. S. Moseley, S. Nibarger, J. P. Niemack, M. D. Parker, L. P. Shirokoff, E. Simon, S. M. Staggs, S. T. Ullom, J. N. U-Yen, K. Visnjic, C. Wollack, E. Yoon, K. W. Young, and E. Y. Zhao, "Optical efficiency of feedhorn-coupled TES polarimeters for next-generation CMB instruments," in *Proc. SPIE*, 2010, vol. 7741, pp. 774122-1–774122-10.

[9] J. Gao, A. Vayonakis, O. Noroozian, J. Zmuidzinas, P. K. Day, and H. G. Leduc, "Measurement of loss in superconducting microstrip at millimeter-wave frequencies," in *Proc. AIP Conf.*, 2009, vol. 1185, pp. 164–167.

[10] W. A. Phillips, "Two-level states in glasses," *Rep. Prog. Phys.*, vol. 50, no. 12, pp. 1657–1708, Dec. 1987.

[11] P. W. Anderson, B. I. Halperin, and C. M. Varma, "Anomalous low-temperature thermal properties of glasses and spin glasses, [Ultrasonic attenuation and magnetic impurity systems]," *Philos. Mag.*, vol. 25, no. 1, pp. 1–9, Jan. 1972.

[12] S. Hunklinger and W. Arnold, *Physical Acoustics*. New York, NY, USA: Academic, 1976, ch. 3, p. 155.

[13] E. M. George, P. Ade, K. A. Aird, J. E. Austermann, J. A. Beall, D. Becker, A. Bender, B. A. Benson, L. E. Bleem, J. Britton, J. E. Carlstrom, C. L. Chang, H. C. Chiang, H. M. Cho, T. M. Crawford, A. T. Crites, A. Datesman, T. de Haan, M. A. Dobbs, W. Everett, A. Ewall-Wice, N. W. Halverson, N. Harrington, J. W. Henning, G. C. Hilton, W. L. Holzapfel, S. Hoover, N. Huang, J. Hubmayr, K. D. Irwin, M. Karfunkle, R. Keisler, J. Kennedy, A. T. Lee, E. Leitch, D. Li, M. Lueker, D. P. Marrone, J. J. McMahon, J. Mehl, S. S. Meyer, J. Montgomery, T. E. Montroy, J. Nagy, T. Natoli, J. P. Nibarger, M. D. Niemack, V. Novosad, S. Padin, C. Pryke, C. L. Reichardt, J. E. Ruhl, B. R. Saliwanchik, J. T. Sayre, K. K. Schaffer, E. Shirokoff, K. Story, C. Tucker, K. Vanderlinde, J. D. Vieira, G. Wang, R. Williamson, V. Yefremenko, K. W. Yoon, and E. Young, "Performance and on-sky optical characterization of the SPTpol instrument," in *Proc. SPIE*, 2012, vol. 8452, p. 845 21F.